

Time-Delay Feedback Neural Network for Fast-Moving Small Target Discrimination Against Complex Dynamic Environments

Hongxin Wang, Huatian Wang, Jiannan Zhao, Cheng Hu, Jigen Peng and Shigang Yue, *Senior Member, IEEE*

Abstract—Discriminating small moving objects in complex visual environments is a significant challenge for autonomous micro robots that are generally limited in computational power. Relying on well-evolved visual systems, flying insects can effortlessly detect mates and track prey in rapid pursuits, despite target sizes as small as a few pixels in the visual field. Such exquisite sensitivity for small target motion is known to be supported by a class of specialized neurons named as small target motion detectors (STMDs). The existing STMD-based models normally consist of four sequentially arranged neural layers interconnected through feedforward loops to extract motion information about small targets from raw visual inputs. However, feedback, another important regulatory circuit for motion perception, has not been investigated in the STMD pathway and its functional roles for small target motion detection are not clear. In this paper, we propose a STMD-based neural network with feedback connection (Feedback STMD), where the network output is temporally delayed, then fed back to lower layers to mediate neural responses. We compare the properties of the model with and without the time-delay feedback loop, and find it shows preference for small targets moving at high velocities. Extensive experiments suggest that the Feedback STMD achieves superior detection performance for fast-moving small targets, while significantly suppresses background false positives with lower velocities in comparison to the existing STMD-based models.

Index Terms—Neural modeling, visual system model, small target motion detection, time-delay feedback, complex background.

I. INTRODUCTION

IMAGES of real-world moving objects could change significantly due to constantly varying distance, position, orientation, shape, occlusion, and lighting conditions [1]. The ability to robustly detect visual motion of interested objects is important for intelligent robots, especially for those executing monitoring and tracking tasks in complex dynamic environments [2]–[4]. To react promptly and hold a dominant position in interaction/competition, artificial visual systems often need to detect moving objects as early and as far as possible, for example, early warning of incoming unmanned

This work was supported in part by EU HORIZON 2020 Project STEP2DYNA under Grant 691154, in part by EU HORIZON 2020 Project ULTRACEPT under Grant 778062, and in part by the National Natural Science Foundation of China under Grant 11771347. (Corresponding authors: Jigen Peng; Shigang Yue.)

Ho. Wang, Hu. Wang, J. Zhao, C. Hu and S. Yue are with the Computational Intelligence Lab, School of Computer Science, University of Lincoln, Lincoln LN6 7TS, U.K. (email: howang@lincoln.ac.uk, syue@lincoln.ac.uk).

J. Peng is with the School of Mathematics and Information Science, Guangzhou University, Guangzhou 510006, China (email: jgpeng@gzhu.edu.cn).



Fig. 1. Example of an UAV in the distance where the UAV and its surrounding region are enlarged in the red box [5].

aerial vehicles (UAVs) at a great distance. Since the objects are distant from the visual sensors, they usually appear as small dim speckles in images with only one or a few pixels in size let alone other visual features, as shown in Fig. 1. Small target¹ motion detection aims to not only identify the locations and velocities of small targets, but also discriminate them from large independently moving objects against heavily cluttered backgrounds.

Small target motion detection has a wide variety of real-world applications such as safe navigation in unknown complex environments [6], video surveillance over a wide area [7], and potential danger warning for advanced autonomous driving [8]. However, detecting small moving targets in complex dynamic environments is much more challenging than large object detection. Traditional motion detection methods [9]–[13] indeed perform well on objects with high resolution, clear appearance and structure, such as pedestrians, bikes, and vehicles. However, they are always powerless for targets as small as a few pixels – because visual features such as texture, color, shape, and orientation, are difficult to identify in such small sizes and cannot be used for motion detection. Moreover, small targets are generally with low resolution and unclear boundaries, which make them easily buried in cluttered backgrounds. Finally, free motion of camera compounded with jitters may bring further difficulties to motion discrimination. Effective solutions to detect small target motion against cluttered moving backgrounds are still rare so far.

Insights from visual neuroscience have led to valuable guidance toward the design of artificial visual systems for small target detection [14]–[17]. Given the evolutionary advantage

¹Small targets refer to objects of interest that appear as small dim speckles in images due to long observation distances. Their sizes may vary from 1 pixel to a few pixels, or equivalent to $1^\circ - 3^\circ$ in visual field preferably.

over millions of years, insects have demonstrated remarkable abilities to detect small target motion in terms of accuracy, efficiency, and robustness. For example, dragonflies can track and intercept small flying prey or mates with limited neural resources while achieving extremely high 97% successful capture rate [18]. The excellent sensitivity of insects for small target motion, as indicated in biological research [19]–[24], comes from a class of specialized neurons called small target motion detectors (STMDs). Specifically, the STMD neurons are strongly excited by small targets occupying $1^\circ - 3^\circ$ of the visual field. However, the neural responses to large bars (typically $> 10^\circ$) or background movements represented by wide-field grating stimuli, are much weaker or fall to spontaneous levels. In addition, the STMD neurons respond robustly against highly complex environments even in the presence of background motion. Such superior neural properties are particularly desirable in developing artificial visual systems for detecting small target motion robustly and computationally efficiently.

Some effort has been devoted to proposing quantitative STMD-based models such as elementary STMD (ESTMD) [25], directionally selective STMD (DSTMD) [26], cascaded models [27]–[29], and STMD Plus [30]. They are featured with a feedforward processing hierarchy to transform raw visual inputs into strong responses to small moving targets. Despite the success of these feedforward models in small target motion detection, accumulated evidences suggest that feedback is also critical for animals' visual perception processes [31]–[33]. While feedforward loops convey visual signals, feedback circuits modulate feature extraction in early layers according to prior knowledge and internal state [34]. Specifically, they can exert positive and/or negative control over lower-layer neurons to enhance neural responses, and suppress distracting signals simultaneously [35], [36].

Feedback mechanism has been proven useful in a number of computer vision tasks, such as saliency detection [37], pose estimation [38], object recognition [39], and visual segmentation [40]. Biological research has also identified various feedback loops in insects' visual systems [41]–[44]. However, it has not been deeply explored in the STMD modeling for small target motion detection. In this paper, we propose a STMD-based model with time-delay feedback named Feedback STMD, to reveal its critical role in discriminating small targets against cluttered moving backgrounds. We conduct systematic analysis as well as extensive experiments, and the results show that the Feedback STMD largely suppresses slow-moving background false positives, whereas maintains significant responses to small targets with higher velocities.

The rest of this paper is organized as follows. Section II provides an overview of the current related research in motion detection and feedback mechanism. Section III presents the proposed Feedback STMD model. Section IV reports the experimental results as well as performance comparisons against the existing models on both synthetic and real-world data sets. Finally, Section V concludes this paper and highlights potential directions for future work.

II. RELATED WORK

In this section, we first review the STMD-based models, then describe feedback mechanism and its applications, finally discuss traditional motion detection approaches.

A. STMD-based Models

STMDs [19]–[24] are a class of widely investigated motion-sensitive neurons that respond most strongly to small moving targets. Several attempts have been made to develop the STMD-based models for small target motion detection. Wiederman *et al.* [25] proposed a computational model named ESTMD to simulate size selectivity of the STMD neurons. The presence of small moving target is detected by the correlation of laterally inhibited luminance-change signals at each pixel. However, the ESTMD does not show direction selectivity and cannot estimate motion direction. To address these issues, two directionally selective models were developed, including DSTMD [26] and cascaded models [27]–[29], where direction selectivity is introduced by correlating signals from two different pixels while motion direction is estimated by a population vector algorithm. Wang *et al.* [30] proposed a STMD Plus model to explore the combination of motion information with directional contrast for filtering out small-target-like background features. The above computational models all process visual signals in a feedforward manner. However, feedback loops which significantly outnumber feedforward connections in insects' visual systems [45], have not been systematically investigated in the STMD neural modeling.

B. Feedback Mechanism

Feedback is a ubiquitous regulatory circuit in insects' visual systems, which mediates lower-layer neural responses by bringing back higher-level semantic information [41]. For example, fruit flies are capable of fine tuning motor behavior using visual feedback during chasing mates or tracking prey [42]; praying mantids deliver binocular disparity feedback to the optic lobes to modulate stereo vision [43]; visual selective attention mechanisms of honeybees involve feedback from the central brain [44].

Over the past decade, feedback mechanisms have been successfully embedded into artificial neural networks to accomplish a variety of visual tasks, such as saliency detection [37], pose estimation [38], object recognition [39], and visual segmentation [40]. In addition, they are also extensively used in control theory to solve the stability problem of nonlinear systems [46]–[48]. Although feedback mechanisms have achieved great success in improving the systems' performances, little work has been done to model them in the STMD neural pathways and their role in small target motion detection is unclear.

C. Traditional Motion Detection Methods

Traditional motion detection can be generally categorized into appearance-based approaches [7], [9], [10] and motion-based approaches [11]–[13]. The former extracts low-to-high level visual features to classify moving objects using machine

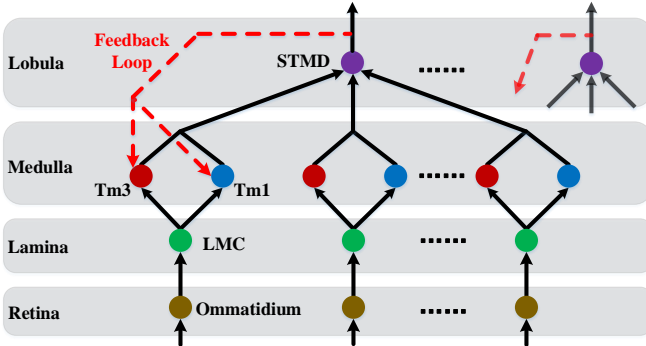


Fig. 2. Wiring sketch of the proposed Feedback STMD model. It consists of four neural layers, including retina, lamina, medulla and lobula (from bottom to top). Each layer contains a number of specific neurons denoted by colored circular nodes. The STMDs interact with the medulla neurons (Tm1 and Tm3) through feedforward and feedback loops. Note that only one feedback loop is presented here for clarity.

learning algorithms, while the latter computes optical flow or temporal luminance change for each pixel to segment moving regions from the background. These methods have excellent detection performance for objects that are sufficiently large and with discriminative visual features in individual images. Nevertheless, they usually fail to detect small targets moving against cluttered backgrounds. This is because visual features are difficult to identify from targets' poor-quality appearance in extremely small sizes [8]. In addition, these methods always suffer from a large number of false positives in the presence of background motion, as small moving targets could be submerged among pixel errors when applying background motion compensation [9].

III. METHODS AND FORMULATIONS

The proposed Feedback STMD model is composed of four sequentially arranged neural layers – retina, lobula, medulla, and lobula, as illustrated in Fig. 2. Each layer contains a number of specialized visual neurons coordinated together to detect small target motion against dynamic complex environments. Specifically, visual information is received by ommatidia [49], then fed into large monopolar cells (LMCs) [50] to calculate luminance change over time. The output of the LMCs is further processed by medulla neurons (Tm1 and Tm3) [51] in parallel, and finally integrated in the STMDs to discriminate small moving targets. The STMDs propagate their outputs to the medulla neurons via feedback loops to mediate neural responses to various visual stimuli. Fig. 3 shows the schematic of the proposed Feedback STMD model, and its formulation will be described in the following subsections.

A. Retina Layer

The retina layer is built from thousands of individual ommatidia that serve as luminance receptors to capture visual information from the external environment. In the proposed model, the ommatidia are arranged in matrix form to receive an entire image frame as input [see Fig. 3]. Each neuron is designed as a Gaussian filter in spatial domain to smooth the luminance signal of each pixel. Formally, we denote the input

image sequence as $I(x, y, t) \in \mathbb{R}$, where x, y and t stand for spatial and temporal coordinates, respectively. The output of an ommatidium $P(x, y, t)$ is defined by the convolution of $I(x, y, t)$ with a Gaussian function $G_{\sigma_1}(x, y)$, namely,

$$P(x, y, t) = \iint I(u, v, t)G_{\sigma_1}(x - u, y - v)dudv \quad (1)$$

$$G_{\sigma_1}(x, y) = \frac{1}{2\pi\sigma_1^2} \exp\left(-\frac{x^2 + y^2}{2\sigma_1^2}\right) \quad (2)$$

where σ_1 is standard deviation of the Gaussian function.

To clearly visualize the signal processing of the proposed model, we illustrate the neural outputs to a dark small moving target in Fig. 4. When the small target passes through the pixel (x_0, y_0) , the output of the ommatidium first declines between 15 ms and 20 ms, then gradually goes up to the original level in the next period (20 to 25 ms), as shown in Fig. 4(a). It should be pointed out that the decrease and increase of the ommatidium output are induced by the arrival and departure of the small target, respectively.

B. Lamina Layer

As can be seen from Fig. 3, the output of the ommatidia forms the input to the LMCs in the lamina layer, each of which is modeled as a band-pass filter to compute luminance change at each pixel with respect to time. The impulse response of the temporal band-pass filter $H(t)$ is defined as the difference of two Gamma kernels [52], that is,

$$H(t) = \Gamma_{n_1, \tau_1}(t) - \Gamma_{n_2, \tau_2}(t) \quad (3)$$

$$\Gamma_{n, \tau}(t) = (nt)^n \frac{\exp(-nt/\tau)}{(n-1)! \cdot \tau^{n+1}} \quad (4)$$

where $\Gamma_{n, \tau}(t)$ denotes Gamma kernel with order n and time constant τ . By convolving $H(t)$ with the ommatidium output $P(x, y, t)$, we have the output of the LMC $L(x, y, t)$

$$L(x, y, t) = \int P(x, y, s)H(t - s)ds. \quad (5)$$

The LMC output $L(x, y, t)$ reveals the change of luminance corresponding to pixel (x, y) at time t . More precisely, a positive output suggests luminance increase, whereas a negative one means luminance decrease, as shown in Fig. 4(b). It is also worth mentioning that the LMC is unable to discriminate object sizes. In other words, the obtained luminance change signals could result from the motion of an any-size object. To filter out large moving objects, the output of the LMC is feed-forwarded to higher neural layers for further processing.

C. Medulla Layer

Two medulla neurons, including Tm1 and Tm3, directly connect with the LMC and process its output in parallel, as illustrated in Fig. 3. Specifically, the Tm3 neuron is modelled as a half-wave rectifier to pass luminance increase component while block decrease component. Note that the luminance increase and decrease components are also referred to as ON and OFF signals, respectively. Denote the output of Tm3 by $S^{Tm3}(x, y, t)$, then we have

$$S^{Tm3}(x, y, t) = [L(x, y, t)]^+ \quad (6)$$

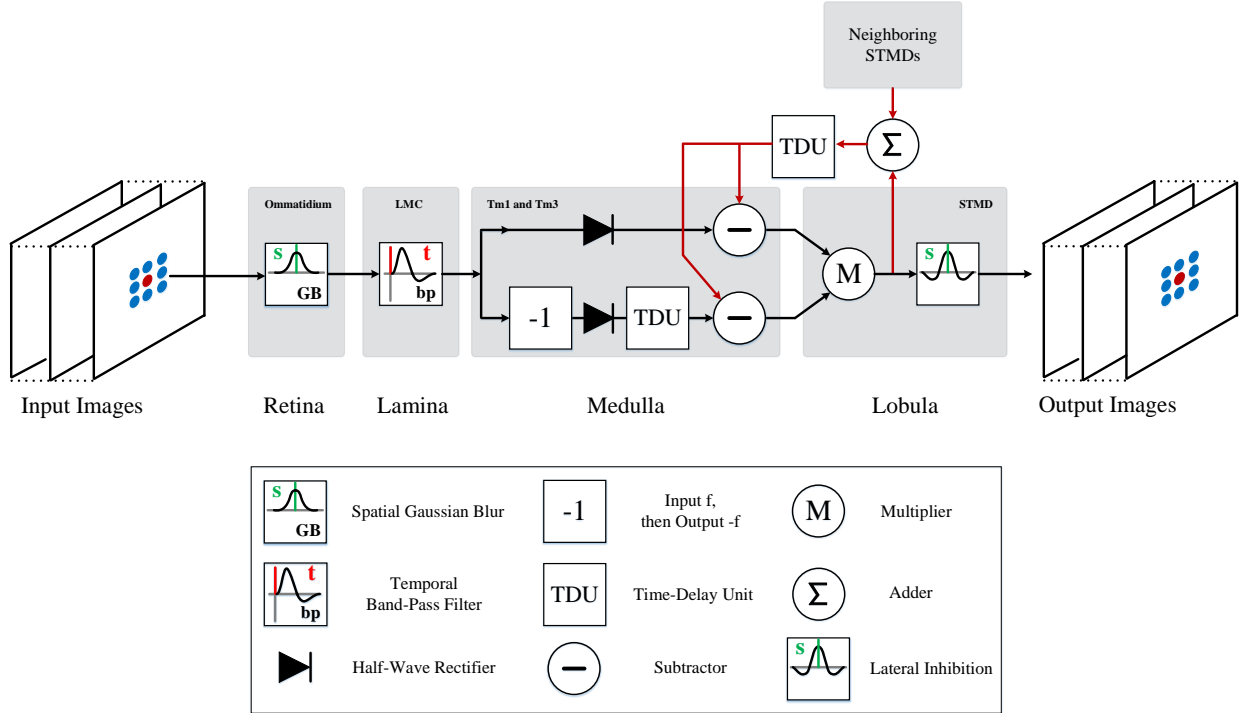


Fig. 3. Schematic of the proposed Feedback STMD model. It takes an entire image frame as input at each time step and extracts motion information about small targets by four feedforward neural layers. The extracted motion information is first temporally delayed, then fed back to the medulla layer to inhibit neural responses to slow-moving objects. We show only one ommatidium, LMC, Tm1, Tm3, and STMD here for better visualization, but they are arranged in matrix form in corresponding neural layers.

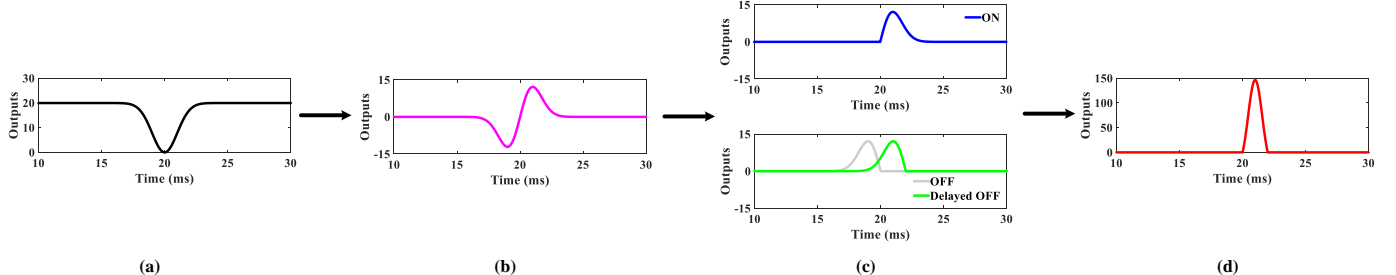


Fig. 4. Neural outputs to a dark small target with respect to time t at a given pixel (x_0, y_0) . (a) Ommatidium output $P(x_0, y_0, t)$. (b) LMC output $L(x_0, y_0, t)$. (c) Tm3 output $S^{Tm3}(x_0, y_0, t)$ and Tm1 output $S^{Tm1}(x_0, y_0, t)$. (d) STMD output $D(x_0, y_0, t)$.

where $[x]^+$ represents $\max(x, 0)$. In contrast, the Tm1 neuron passes luminance decrease component and further temporally delays it by convolution with a Gamma kernel, that is,

$$S^{Tm1}(x, y, t) = \int [-L(x, y, s)]^+ \cdot \Gamma_{n_3, \tau_3}(t - s) ds \quad (7)$$

where $S^{Tm1}(x, y, t)$ denotes the output of Tm1, the time-delay length and time-delay order are determined by the time constant τ_3 and order n_3 of Gamma kernel $\Gamma_{n_3, \tau_3}(t)$, respectively.

As can be seen from Fig. 4(c), the outputs of the Tm3 (ON) and Tm1 (OFF) are aligned properly in the temporal field after applying time delay, where the time-delay length is set as the duration for the small target to pass through the pixel, i.e., the ratio of the target width to its velocity. The aligned ON and OFF signals are further multiplied together to produce a large response to the small moving target [see Fig. 4(d)]. On

the other hand, recent biological studies [35], [36] indicate that the ON- and OFF-type cells may optimize neural coding for object motion using feedback from higher neural layers. Inspired by the biological finding, the proposed model exerts feedback control over the medulla neurons to regulate their responses to different moving objects, as displayed in Fig. 3. For convenience of description, the whole feedback loop is formulated in the next subsection.

D. Lobula Layer

It can be observed from Fig. 3 that the STMD integrates the two medulla neural outputs at the same pixel for small target motion detection. More precisely, the medulla neural outputs first subtract a feedback signal, and are then recombined together by multiplication to generate a significant response,

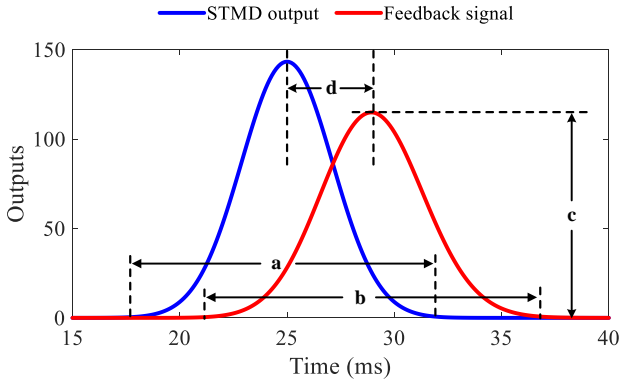


Fig. 5. The STMD output and feedback signal with respect to time t at a given pixel (x_0, y_0) . The letter a represents the response duration of the STMD output, while the letters b , c , and d denote the response duration, the strength, and time-delay length of the feedback signal, respectively.

that is,

$$D(x, y, t) = \left\{ S^{\text{Tm}3}(x, y, t) - F(x, y, t) \right\} \times \left\{ S^{\text{Tm}1}(x, y, t) - F(x, y, t) \right\} \quad (8)$$

where $D(x, y, t)$ denotes the output of the STMD neuron, and $F(x, y, t)$ represents the feedback signal. In the feedback direction, the outputs of the central STMD and its neighbors are temporally delayed by convolving with a Gamma kernel, then propagated to the medulla layer as feedback signals, so we have

$$F(x, y, t) = \alpha \cdot \int \left\{ D(x, y, s) + E(x, y, s) \right\} \cdot \Gamma_{n_4, \tau_4}(t - s) ds \quad (9)$$

where α is a feedback constant, $E(x, y, t)$ stands for the weighted summation of the neighboring STMD neural outputs, and n_4 and τ_4 are the order and time constant of Gamma kernel $\Gamma_{n_4, \tau_4}(t)$, respectively. Here, we define the weight function as

$$W_e(x, y) = \frac{1}{2\pi\eta^2} \exp\left(-\frac{x^2 + y^2}{2\eta^2}\right) \quad (10)$$

where η is a constant. Then, $E(x, y, t)$ can be given by

$$E(x, y, t) = \iint \left\{ S^{\text{Tm}3}(u, v, t) \times S^{\text{Tm}1}(u, v, t) \right\} \times W_e(x - u, y - v) du dv \quad (11)$$

To reveal the role of the time-delay feedback, we first analyse the STMD output and its feedback signal. As illustrated in Fig. 5, the STMD output is significantly greater than zero during a certain time period called response duration². The response duration of the STMD is determined by the time length for the object to completely cover the pixel, i.e., the reciprocal of the object's velocity $1/v$. The longer response duration means the more time for the object to cover the pixel, and therefore the lower object's velocity. Here we formulate this relation as $a = f(1/v)$ where $f(\cdot)$ is an increasing function. The feedback signal is the delayed version of the

²Response duration represents the time elapsing between onset of the response and its termination, i.e., recovering to the original level.

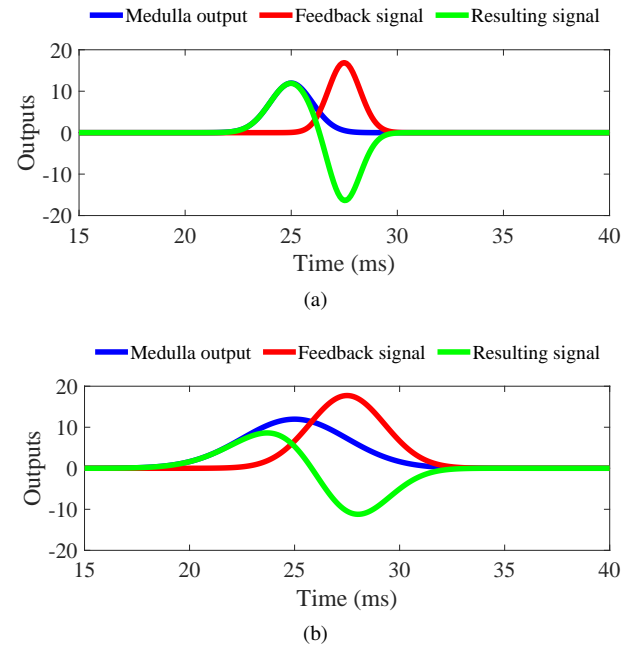


Fig. 6. Feedback on medulla neurons with (a) short response duration, and (b) long response duration, where the feedback constant, order, and time-delay length of the feedback loop are fixed. Note that the longer response duration always means the lower object's velocity. The medulla output with short response duration maintains its maximum after feedback, whereas the long-response-duration output is strongly suppressed.

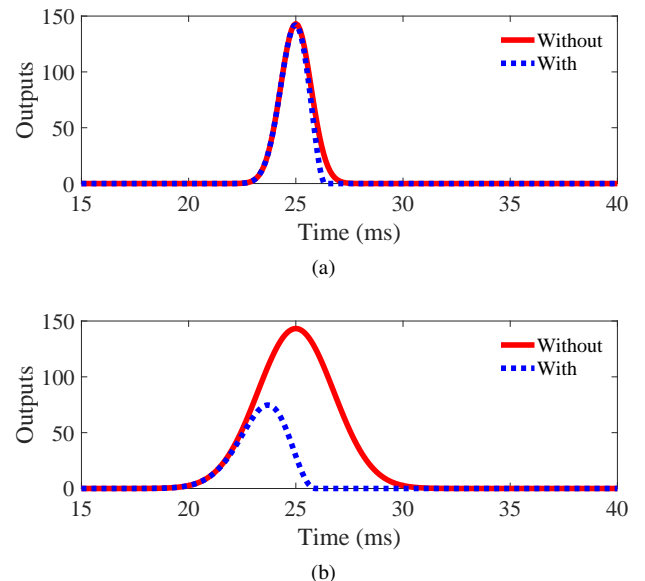


Fig. 7. Outputs of the STMD with and without feedback. (a) Short response duration. (b) Long response duration. The STMD output with short response duration maintains its maximum after feedback, whereas the long-response-duration output is strongly suppressed.

STMD output, where its response duration, strength, and time-delay length are controlled by the parameters n_4 , α , and τ_4 , respectively [see (9) and Fig. 5]. Moreover, the response duration of the feedback signal is larger than that of the STMD (i.e., $b > a$), according to the convolution property.

We further compare neural outputs with different response durations after applying the negative feedback, as shown in Fig. 6 and 7. Obviously, if the time-delay length is greater than

TABLE I
PARAMETERS OF THE PROPOSED FEEDBACK STMD MODEL

Eq.	Parameters
(2)	$\sigma_1 = 1$
(3)	$n_1 = 4, \tau_1 = 8, n_2 = 16, \tau_2 = 32$
(7)	$n_3 = 9, \tau_3 = 45$
(9)	$\alpha = 1, n_4 = 10, \tau_4 = 25$
(10)	$\eta = 1.5$
(15)	$A = 1, B = 3$
(16)	$\sigma_2 = 1.5, \sigma_3 = 3, e = 1, \rho = 0$

half of the response duration of the feedback signal, i.e., $d > b/2$, the outputs of the medulla neurons and the STMD output will maintain their maximums unchanged after subtracting the feedback signal [see Fig. 6(a) and 7(a)]. Thus, we have

$$d > \frac{b}{2} > \frac{a}{2} = \frac{f(1/v)}{2} \quad (12)$$

$$v > \frac{1}{f^{-1}(b)} > \frac{1}{f^{-1}(2d)} \quad (13)$$

where $f^{-1}(\cdot)$ is the inverse function of $f(\cdot)$. These two equations suggest that when the time-delay length is fixed, the feedback loop has minor effect on the neural responses to objects with velocity larger than $1/f^{-1}(2d)$; on the contrary, if $v < 1/f^{-1}(2d)$, the medulla neural outputs as well as the STMD output will be significantly suppressed by the feedback signal [see Fig. 6(b) and 7(b)]. Note that $1/f^{-1}(b)$ and $1/f^{-1}(2d)$ can be tuned by the three parameters α , n_4 , and τ_4 , which will be further discussed in Section IV-D. The above analysis indicates that the time-delay feedback loop shows preference for fast-moving objects, which could be a support for the biological finding that animals' visual systems generally allocate more attention for fast-moving objects than those moving at lower velocities [53]–[55].

As this stage, the STMD can eliminate slow-moving objects by the proposed time-delay feedback, while maintain significant responses to those with higher velocities regardless of their size. To suppress responses to large objects, we further convolve the STMD output $D(x, y, t)$ with a lateral inhibition kernel $W_s(x, y)$, namely,

$$Q(x, y, t) = \iint D(u, v, t) W_s(x - u, y - v) du dv \quad (14)$$

where $Q(x, y, t)$ denotes the laterally inhibited output, $W_s(x, y)$ is defined as

$$W_s(x, y) = A \cdot [g(x, y)]^+ + B \cdot [g(x, y)]^- \quad (15)$$

$$g(x, y) = G_{\sigma_2}(x, y) - e \cdot G_{\sigma_3}(x, y) - \rho \quad (16)$$

where $[x]^+$ and $[x]^-$ represent $\max(x, 0)$ and $\min(x, 0)$, respectively, A, B, e and ρ are constant. To identify the locations of small targets, the model output $Q(x, y, t)$ is compared with a detection threshold λ . If $Q(x, y, t) > \lambda$, the location (x, y) is considered as a positive detection. In other words, we believe that a small target is detected at the location (x, y) .



Fig. 8. Input image at time $t_0 = 750$ ms where a small target (the black block) is moving against the cluttered natural background. The velocity of the small target is set to 250 pixels/s, whereas that of the background is lower (150 pixels/s). Arrow V_B denotes the motion direction of the background. The tree is considered as a large object moving with the background at the same velocity.

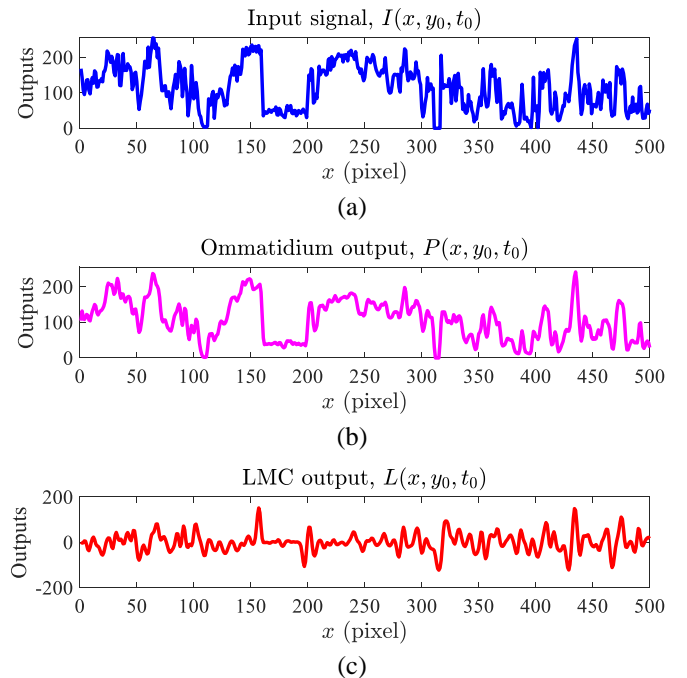


Fig. 9. Neural outputs with respect to x for the given $y_0 = 125$ pixels and time $t_0 = 750$ ms. (a) Input luminance signal $I(x, y_0, t_0)$. (b) Ommatidium output $P(x, y_0, t_0)$. (c) LMC output $L(x, y_0, t_0)$.

IV. EXPERIMENTAL RESULTS AND DISCUSSIONS

A. Experimental Setup

1) *Data Sets*: We evaluate the proposed Feedback STMD on two publicly available data sets, including Vision Egg [56] and RIST [57]. The Vision Egg data set includes a number of synthetic image sequences, each of which displays a computer generated small target (i.e., black block) moving against real background images. The synthetic videos cover a wide variety of background and target types with different parameters, such as luminance, velocity, and size. Their sampling frequency is set to 1000 Hz, while resolution is 500 pixels (in horizontal) by 250 pixels (in vertical). The RIST data set consists of 16 videos captured in real-world environments using an action camera (GoPro Hero 6) at 240 fps. Each video holds an object with size ranging between 3×3 and 15×15 pixels, and contains various types of challenging scenarios, such as highly cluttered

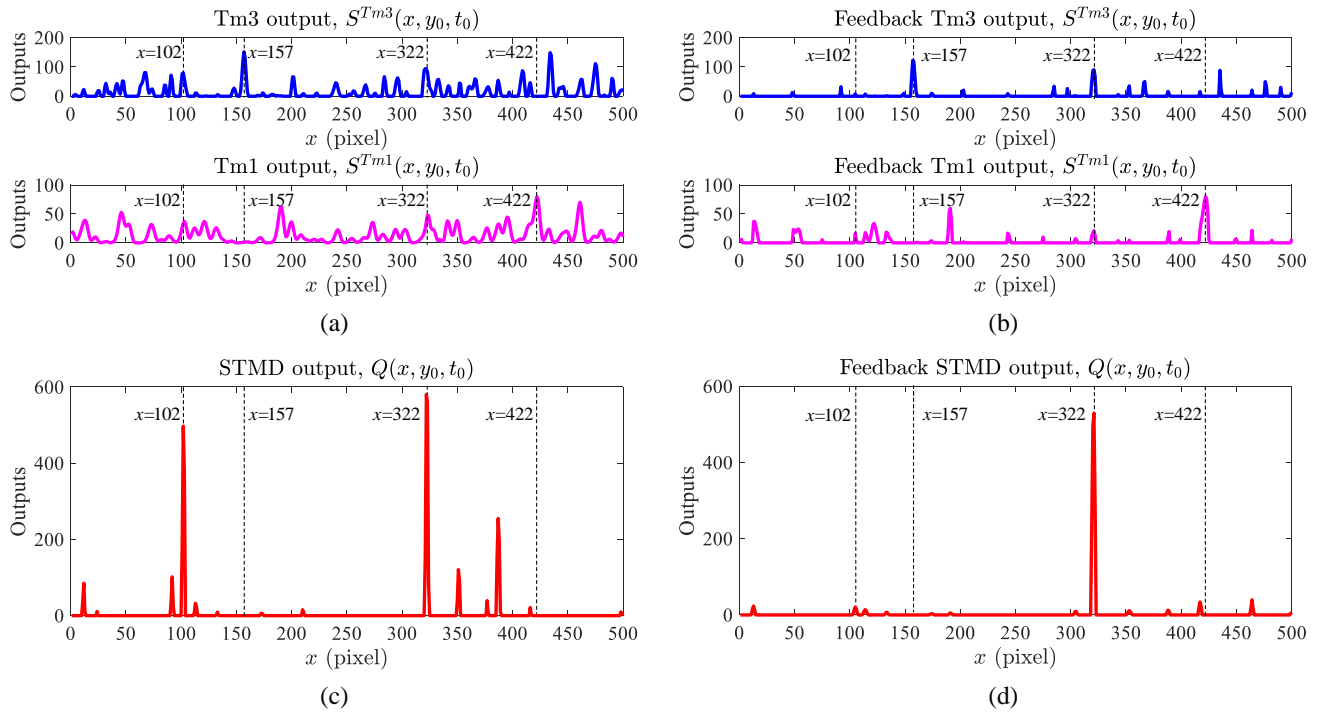


Fig. 10. Comparison of neural outputs with and without feedback. Two medulla neural outputs (a) without and (b) with feedback, and the STMD output (c) without and (d) with feedback. The STMD with feedback effectively suppress responses to background false positives.

background, low contrast object, sudden camera motion, and bad weather conditions.

2) *Evaluation Criteria*: We employ detection rate and false alarm rate to quantitatively evaluate the performance of the proposed Feedback STMD as well as other STMD-based models. The two metrics can be calculated as

$$D_R = \frac{\text{number of true positives}}{\text{number of actual targets}} \quad (17)$$

$$F_A = \frac{\text{number of false positives}}{\text{number of images}} \quad (18)$$

where D_R and F_A denote detection rate and false alarm rate, respectively. A detection is counted as true positive if its distance to the ground truth is smaller than a threshold (5 pixels).

3) *Implementation*: We implement the proposed Feedback STMD model in the Matlab environment on a laptop with 2.20GHz Intel Core i7 CPU and 16GB memory. As in [26], we properly tune the parameters of the four feed-forward layers based on the preferred velocity and size of small targets, while those of the feedback loop are determined by the analysis in Section III-D and sensitivity study in Section IV-D. Table I presents the parameter settings for the experimental results.

B. Effectiveness of the Time-Delay Feedback

To validate the effectiveness of the time-delay feedback in suppressing slow-moving objects, we compare the neural outputs with and without feedback. Fig. 8 shows the input image at time $t_0 = 750$ ms where a small target is moving against cluttered background. For better visualization and comparison of neural processing, we first set $y_0 = 125$ pixels then present

the input luminance signal $I(x, y_0, t_0)$ with respect to x as well as its resulting neural outputs in Fig. 9 and 10. Since the time-delay feedback is only applied to medulla layer, it does not affect the ommatidium output $P(x, y_0, t_0)$ and LMC output $L(x, y_0, t_0)$, shown in Fig. 9(b) and (c), respectively. As can be seen, the ommatidium output is a smooth blur resembling of the input luminance signal, whereas the LMC output reflects the luminance change over time at each pixel. Specifically, a positive LMC output at a pixel x means luminance increase while a negative output represents luminance decrease.

We further compare the outputs of medulla neurons and STMD neuron with and without feedback. Fig. 10(a) displays the two medulla neural outputs without feedback, where the Tm3 output $S^{Tm3}(x, y_0, t_0)$ is the positive half of the LMC output while the Tm1 output $S^{Tm1}(x, y_0, t_0)$ is a time-delay version of the negative half. These two medulla neural outputs are multiplied together then laterally inhibited to define the STMD neural output $Q(x, y_0, t_0)$ in Fig. 10(c). It can be observed that the STMD exhibits a strong response at $x = 322$, i.e., the location of the small target, whereas the responses at other pixels such as $x = 157, 422$ are close to 0. This is because the two maximums of the medulla neural outputs at $x = 322$ are properly aligned by time delay [see Fig. 10(a)], which finally results in a significant STMD output after multiplication and lateral inhibition. However, the outputs of the medulla neurons at the pixels $x = 157, 422$ are unable to achieve precise alignment, consequently leading to extremely low responses of the STMD neurons. Note that $x = 157$ corresponds to the location of the tree which is regarded as a big object in the input image.

On the other hand, we realize that the STMD cannot

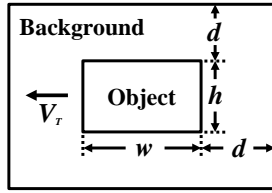


Fig. 11. Illustration of an object and its neighboring background rectangle, where V_T , w , h , and d denote motion direction of the object, object width, object height, and a constant, respectively.

completely filter out false positives against the cluttered background by the signal alignment as well as lateral inhibition. As shown in Fig. 10(c), the STMD still responds strongly at some background pixels, such as $x = 102$. The proposed time-delay feedback loop is able to suppress these background false positives utilizing velocity difference between the small target and background. Since the background is moving at a lower velocity (150 pixels/s) compared to the small target (250 pixels/s), the medulla neural responses to the background features are strongly inhibited by subtracting the time-delay feedback signal, whereas the responses to the small target can be well maintained, as illustrated in Fig. 10(b). Their resulting STMD output is shown in Fig. 10(d). As can be seen, the STMD with feedback gives the maximal response to the small target ($x = 322$), however, its responses to background features at other pixels are significantly suppressed.

In the above experiment, the time-delay feedback loop demonstrated its ability to improve performance of the STMD for small target motion detection by inhibiting slow-moving background features. Relative motion has been regarded as an important cue for animals to discriminate objects from cluttered environments [58]–[60]. From this perspective, the proposed feedback loop provides a possible explanation for how relative motion information facilitates object discrimination against complex moving backgrounds.

C. Tuning Properties of the Feedback STMD

As revealed in the biological research [19]–[24], the STMD neurons display four distinct tuning properties including velocity selectivity, width selectivity, height selectivity, and Weber contrast sensitivity. To validate the tuning properties of the proposed model, we report the model outputs with respect to different object velocities, widths, heights, and Weber contrast in this subsection. For an object with size of $w \times h$ pixels, the size of its neighboring background rectangle is set as $(w+2d) \times (h+2d)$ where d is a constant (10 pixels), as shown in Fig. 11. Weber contrast measures the luminance difference between the object and its neighboring region, which can be calculated by

$$\text{Weber contrast} = \frac{|\mu_t - \mu_b|}{255} \quad (19)$$

where μ_t denotes average pixel intensity of the object, and μ_b represents average pixel intensity of the neighboring background region. We initialize the four parameters of the object, i.e., velocity, width, height, and Weber contrast, to 250 pixels/s, 5 pixels, 5 pixels, and 1, respectively, then record the

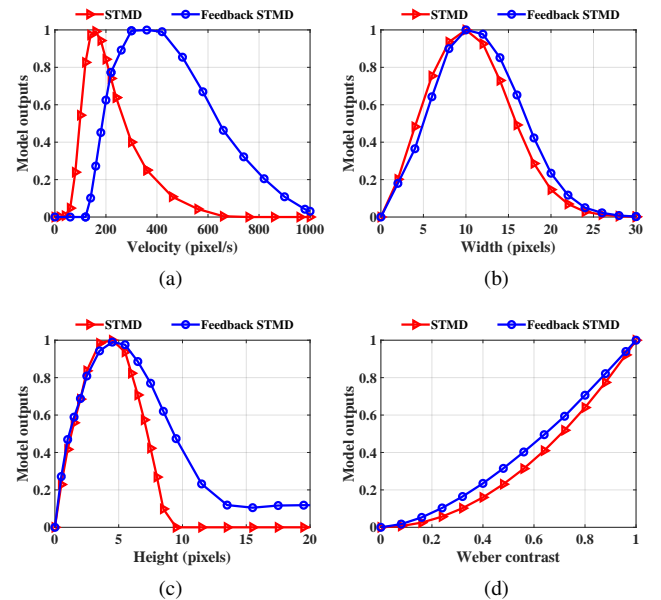


Fig. 12. Outputs of the STMD and Feedback STMD to objects with different (a) velocities, (b) widths, (c) heights, and (d) Weber contrast.

model outputs by changing one of the object parameters while fixing the other three at their initial values.

Fig. 12(a)–(d) shows the outputs of the Feedback STMD model with respect to object velocity, width, height, and Weber contrast, respectively, where the outputs of the STMD (without feedback) is also provided for comparison. As can be seen from Fig. 12(a), the STMD responds significantly to objects with velocities ranging from 50 to 400 pixels/s (output > 0.2), and reaches its maximal output at 150 pixels/s. Note that the interval [50, 400] pixels/s and velocity 150 pixels/s are referred as preferred velocity range and optimal velocity, respectively. Compared to the STMD, the Feedback STMD peaks at a higher velocity 350 pixels/s, and has a much wider range of preferred velocities between 150 and 800 pixels/s. This is because the time-delay feedback loop can largely suppress responses to objects with low velocities (< 200 pixels/s), which finally leads to a significant shift of the preferred velocity range toward high-velocity side. In Fig. 12(b), we can see that both the STMD and Feedback STMD give preference to objects whose widths are lower than 20 pixels, and reach maximum at width = 10 pixels. Moreover, these two models have the same preferred height range (< 10 pixels) as well as the same optimal height (5 pixels), as displayed in Fig. 12(c). It can be observed from Fig. 12(d) that the two models yield higher outputs with the increase of Weber contrast, and finally peak at Weber contrast = 1.

In the above experiment, the model with and without feedback all demonstrate velocity selectivity, width selectivity, height selectivity, and Weber contrast sensitivity. On the other hand, the results also indicate that the time-delay feedback cannot directly affect the presence or absence of the four tuning properties, though it actually changes the optimal velocity and preferred velocity range.

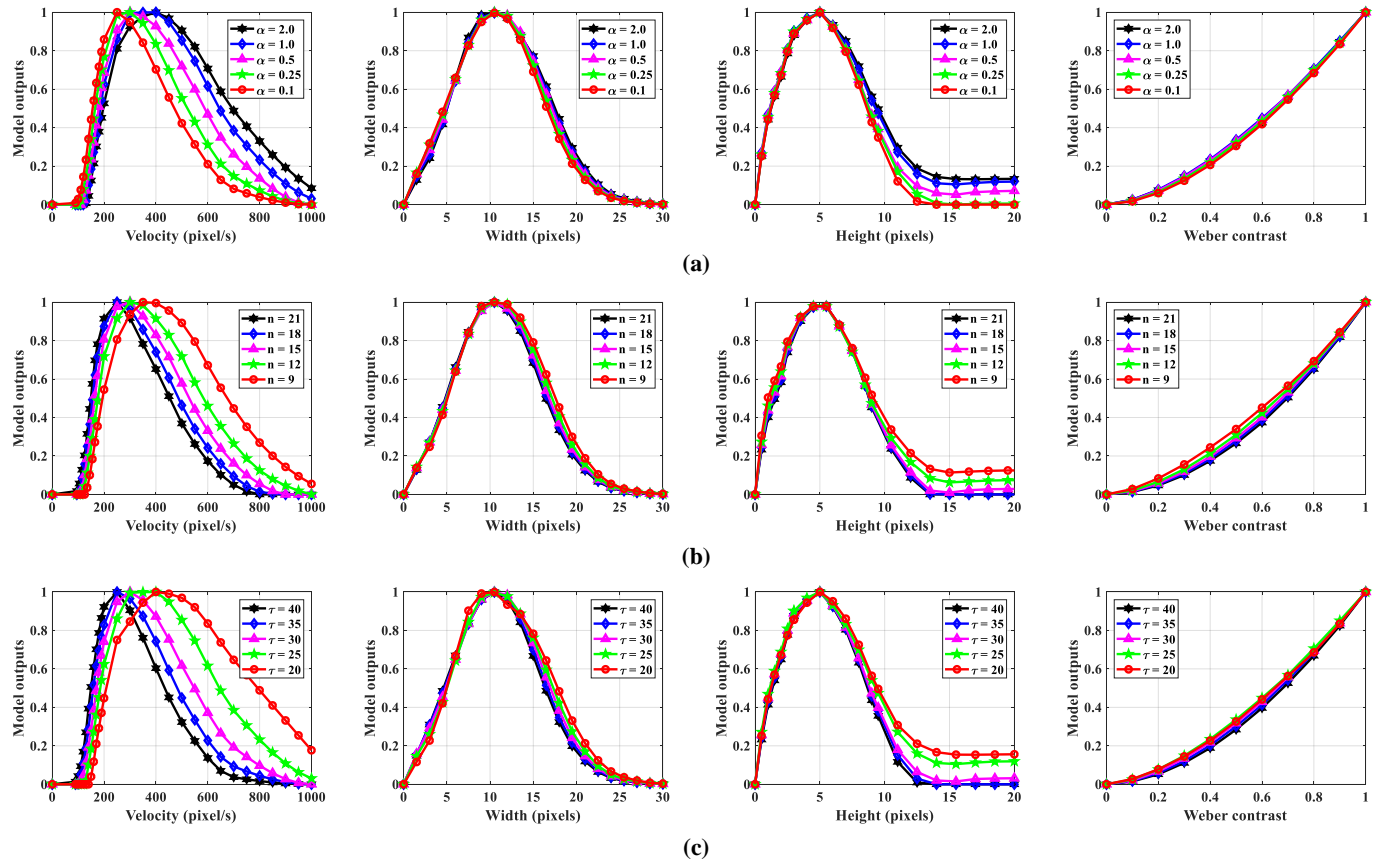


Fig. 13. Tuning properties of the Feedback STMD under (a) different feedback constant α , (b) time-delay order n_4 , and (c) time-delay length τ_4 . The three parameters can adjust the optimal velocity and preferred velocity range, but have minor effect on width selectivity, height selectivity and Weber contrast sensitivity.

D. Parameter Sensitivity Analysis

The time-delay feedback loop is completely determined by three preset parameters, including the feedback constant α , the order n_4 and time constant τ_4 of the Gamma kernel, as indicated in (9). We conduct the parameter sensitivity study in terms of α , n_4 and τ_4 to evaluate their effect on tuning properties of the Feedback STMD.

Let us first study the feedback constant α which is tuned within $\{0.1, 0.25, 0.5, 1, 2\}$. Fig. 13(a) shows the tuning properties of the Feedback STMD with respect to different α . As can be seen, the optimal velocity increases from 250 to 400 pixels/s as the increase of α , and the preferred velocity range is also extended to a much higher value. However, the width selectivity, height selectivity, and Weber contrast sensitivity, are little affected by the change of α . Note that the optimal height (5 pixels) and the preferred height range (< 10 pixels) remain unchanged, though larger α will lead to a slight increase in the model outputs for heights greater than 10 pixels. The reason for the above results is that the parameter α controls the strength of the feedback signal, as illustrated in Fig. 5. The responses to objects with low velocities will be much weaker when subtracting a stronger feedback signal, which finally causes the shift of the optimal velocity to 400 pixels/s.

Next, we study the tuning properties of the Feedback STMD

in regard to different n_4 and τ_4 , which are tuned within $\{9, 12, 15, 18, 21\}$ and $\{20, 25, 30, 35, 40\}$, respectively. The experimental results are shown in Fig. 13(b) and (c). As can be seen, the decrease of n_4 and τ_4 shifts the optimal velocity to a higher value, and significantly broadens the preferred velocity range toward high-velocity side. However, the other three tuning properties are less sensitive to the changes of n_4 and τ_4 . This is because n_4 and τ_4 control the response duration and time-delay length of the feedback signal, respectively [see Fig. 5]. The smaller n_4 (or τ_4) generally means the stronger feedback signal, and therefore the weaker responses to slow-moving objects.

The results shown in Fig. 13, on the other hand, reveal a feasible approach to optimize performance for small target motion detection. Specifically, if the velocity of the small target is estimated in advance, the model's optimal velocity and preferred velocity range can be shifted to closely match the estimated velocity by tuning the parameters of the feedback loop, i.e., α , n_4 , and τ_4 .

E. Comparison with the Existing STMD-based Models

We compare the proposed Feedback STMD with two baseline models, including ESTMD [25] and DSTMD [26], on both synthetic and real data sets in terms of detection rate and false alarm rate. As shown in Table II, the synthetic

TABLE II
DETAILS OF THE SYNTHETIC IMAGE SEQUENCES THAT ARE CATEGORIZED INTO SIX GROUPS IN TERMS OF SIX DIFFERENT IMAGE PARAMETERS.

Image parameter	Initial sequence	Group 1	Group 2	Group 3	Group 4	Group 5	Group 6
Target size (pixels \times pixels)	5×5	$1 \times 1 \sim 15 \times 15$	5×5				
Target luminance	0	0	$0 \sim 75$	0	0	0	0
Target velocity (pixels/s)	250	250	250	$0 \sim 500$	250	250	250
Background velocity (pixels/s)	150	150	150	$0 \sim 500$	$0 \sim 500$	150	150
Background motion direction	rightward	rightward	rightward	rightward	rightward	leftward	rightward
Background Image	Fig.8	Fig.8	Fig.8	Fig.8	Fig.8	Fig.8	Fig.15(a) ~ (c)

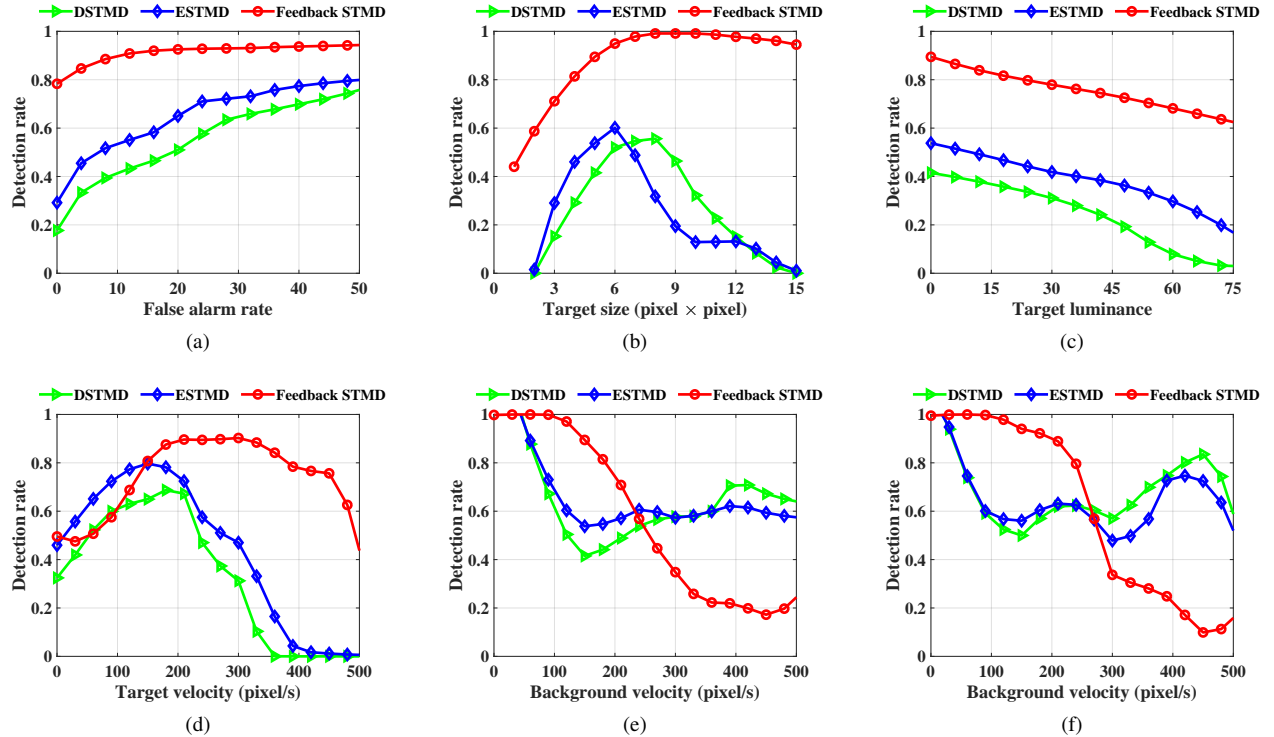


Fig. 14. (a) ROC curves of the Feedback STMD and the two baseline models on the initial image sequence. (b)-(f) Detection rates under the fixed false alarm rate $F_A = 10$ with respect to (b) target size, (c) target luminance, (d) target velocity, (e) background velocity (leftward motion), and (f) background velocity (rightward motion). The Feedback STMD improves detection performances for fast-moving small targets.

image sequences are classified into six groups based on target size, target luminance, target velocity, background velocity, background motion direction, and background images, to study the relations between model performances and the six image parameters. For fair comparison, the baseline models are properly tuned to cover the same preferred velocity range and size range with the STMD [see Fig. 12].

The receiver operating characteristics (ROC) curves of the proposed Feedback STMD and the two baseline models on the initial image sequence are shown in Fig. 14(a). As can be seen, the Feedback STMD yields much better detection performance than the baseline models. Specifically, the detection rate of the Feedback STMD is consistently higher than those of the ESTMD and DSTMD for any false alarm rate. We further report the experimental results on the six groups of image sequences. Fig. 14(b)-(f) displays the detection rates of the three models on the Group 1-5, respectively, where the false alarm rates are all fixed to 10. As shown in Fig. 14(b), the

Feedback STMD achieves the best performance among the three models for different sized targets. The detection rate of the Feedback STMD remains at a high value (> 0.9) when the target size increases from 6×6 to 15×15 pixels. However, the two baseline models all experience a sharp decrease in detection rate to 0, after reaching their maximums at target size = 6×6 pixels. In Fig. 14(c), we can observe that the Feedback STMD consistently outperforms the ESTMD and DSTMD models for different target luminance. It is also worth pointing out that the decrease of target luminance can result in performance degradation of all the models. As can be seen from Fig. 14(d), the Feedback STMD clearly surpasses the baseline models when the target velocity is greater than that of the background (150 pixels/s). Moreover, a higher target velocity will lead to a larger difference of detection rates between the Feedback STMD and the baseline models. This indicates that the larger velocity difference, the more easily small targets can be discriminated from backgrounds. From Fig. 14(e) and (f),

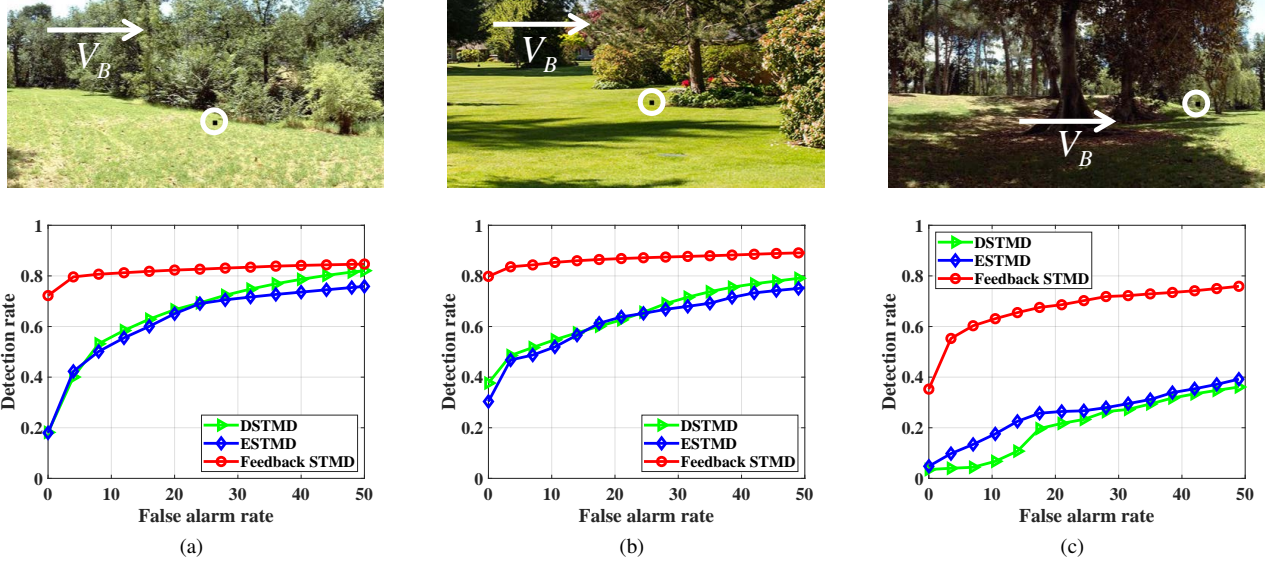


Fig. 15. Background images and ROC curves of the proposed Feedback STMD on the Group 6 in comparison to the ESTMD and DSTMD models. The Feedback STMD outperforms the other two models for different background images.

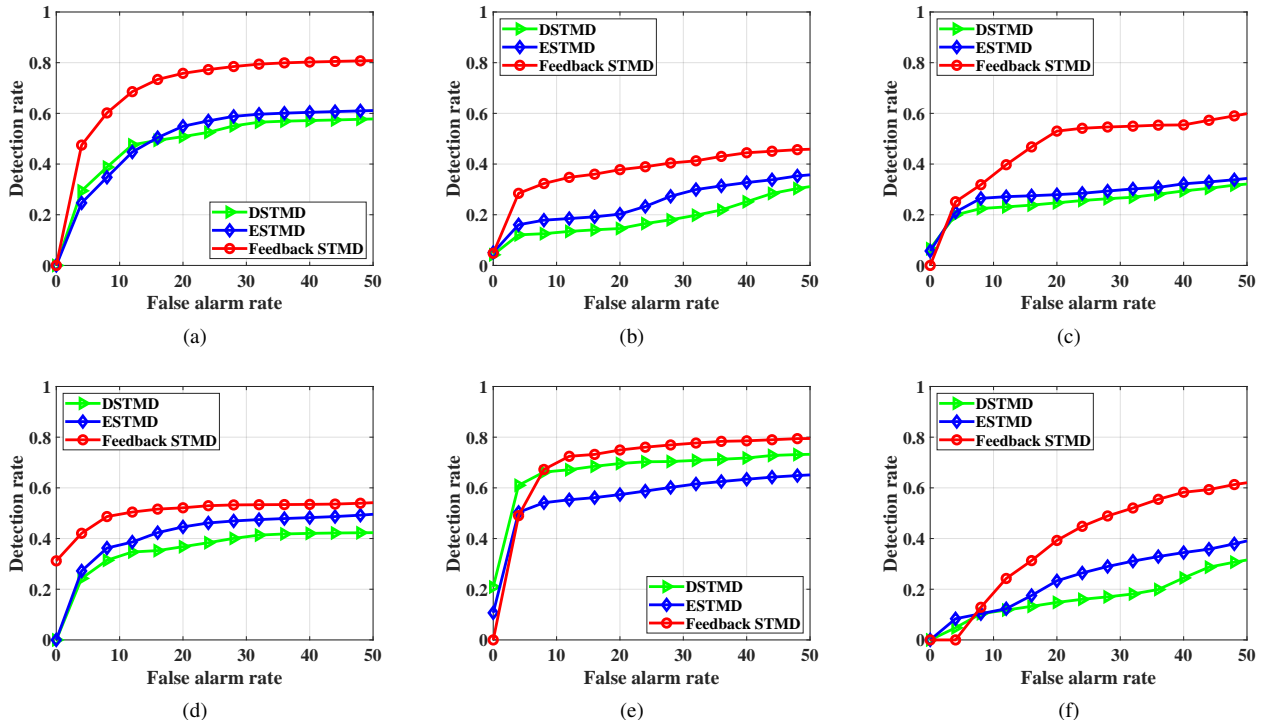


Fig. 16. ROC curves of the proposed Feedback STMD on six real videos in comparison to the ESTMD and DSTMD models. (a) Real video 1 (GX010071). (b) Real video 2 (GX010250). (c) Real video 3 (GX010303). (d) Real video 4 (GX010307). (e) Real video 5 (GX010322). (f) Real video 6 (GX010337). The Feedback STMD achieves better performance than the other two models on all real videos.

we can find that the Feedback STMD significantly improves detection rates when the background moves more slowly than the small target (< 250 pixels/s). However, it performs much worse than the baseline models when the background velocity is higher than that of the small target. The reason for the above results is that the Feedback STMD prefers fast-moving small targets while strongly inhibits objects with low velocities by time-delay feedback. When the background is moving

faster than the small target (> 250 pixels/s), background false positives will receive much weaker suppression from the feedback loop, which consequently leads to the decrease of detection rate. The ROC curves of the proposed Feedback STMD and the baseline models on the Group 6 are shown in Fig. 15. It can be observed that the Feedback STMD achieves much better performance than the ESTMD and DSTMD in all background images.

We evaluate the models on six real videos and report their ROC curves in Fig. 16. The videos are randomly selected from the RIST data set, each of which displays a fast-moving small target against the cluttered background. The corresponding video numbers are given in the caption. As can be seen, the Feedback STMD outperforms the ESTMD and DSTMD on all six videos. Specifically, its detection rate is always higher than those of the other two models for any false alarm rate.

V. CONCLUSION

In this paper, we developed a STMD-based neural network with time-delay feedback (Feedback STMD) to discriminate fast-moving small targets from cluttered background. The proposed model contains four sequentially arranged layers and a time-delay feedback loop. The four neural layers interconnected by feedforward connections are intended to extract motion information about small targets by computing luminance change of each pixel with respect to time. The feedback loop is designed to propagate the extracted motion information to lower neural layers to inhibit slow-moving background false positives. The model with and without feedback were evaluated and compared on the synthetic and real data sets to demonstrate the effectiveness of feedback. Experimental results show that the time-delay feedback can maintain model responses to fast-moving objects, while significantly suppress those with lower velocities. Moreover, it is able to improve detection performance for small targets with velocities higher than that of the complex background. In the future, we will consider other possible feedback types such as time-varying feedback, and explore their self-adaptability for various objects and environments.

REFERENCES

- [1] D. L. Yamins, H. Hong, C. F. Cadieu, E. A. Solomon, D. Seibert, and J. J. DiCarlo, "Performance-optimized hierarchical models predict neural responses in higher visual cortex," *Proc. Natl. Acad. Sci. U.S.A.*, vol. 111, no. 23, pp. 8619–8624, Jun. 2014.
- [2] S. Yue and F. C. Rind, "Redundant neural vision systems-competing for collision recognition roles," *IEEE Trans. Auton. Mental Develop.*, vol. 5, no. 2, pp. 173–186, Apr. 2013.
- [3] B. Hu, S. Yue, and Z. Zhang, "A rotational motion perception neural network based on asymmetric spatiotemporal visual information processing," *IEEE Trans. Neural Netw. Learn. Syst.*, vol. 28, no. 11, pp. 2803–2821, Nov 2016.
- [4] S. Yue and F. C. Rind, "Collision detection in complex dynamic scenes using an Igmd-based visual neural network with feature enhancement," *IEEE Trans. Neural Netw.*, vol. 17, no. 3, pp. 705–716, May 2006.
- [5] [Online], Available: https://www.youtube.com/watch?v=ihg7_RkuLuE&list=FL_OHabe8rogCpinac5KHGYA&index=4&t=360s, accessed Jun. 6, 2019.
- [6] H. D. Escobar-Alvarez, M. Ohradzansky, J. Keshavan, B. N. Ranganathan, and J. S. Humbert, "Bioinspired approaches for autonomous small-object detection and avoidance," *IEEE Trans. Robot.*, vol. 35, no. 5, pp. 1220–1232, Oct. 2019.
- [7] B. Bosquet, M. Mucientes, and V. M. Brea, "Stdnet: A convnet for small target detection," in *Proc. Conf. BMVC*, 2018.
- [8] J. Li, X. Liang, Y. Wei, T. Xu, J. Feng, and S. Yan, "Perceptual generative adversarial networks for small object detection," in *Proc. IEEE Conf. Comput. Vis. Pattern Recognit. (CVPR)*, Jul. 2017, pp. 1222–1230.
- [9] R. LaLonde, D. Zhang, and M. Shah, "Clusternet: Detecting small objects in large scenes by exploiting spatio-temporal information," in *Proc. IEEE Conf. Comput. Vis. Pattern Recognit.*, 2018, pp. 4003–4012.
- [10] A. Rozantsev, V. Lepetit, and P. Fua, "Detecting flying objects using a single moving camera," *IEEE Trans. Pattern Anal. Mach. Intell.*, vol. 39, no. 5, pp. 879–892, May 2017.
- [11] S. Javed, A. Mahmood, S. Al-Maadeed, T. Bouwmans, and S. K. Jung, "Moving object detection in complex scene using spatiotemporal structured-sparse rpca," *IEEE Trans. Image Process.*, vol. 28, no. 2, pp. 1007–1022, Oct. 2018.
- [12] D. Fortun, P. Bouthemy, and C. Kervrann, "Optical flow modeling and computation: a survey," *Comput. Vis. Image Underst.*, vol. 134, pp. 1–21, May 2015.
- [13] I. Saleemi and M. Shah, "Multiframe many-many point correspondence for vehicle tracking in high density wide area aerial videos," *Int. J. Comput. Vision*, vol. 104, no. 2, pp. 198–219, Sep. 2013.
- [14] H. Wang, Q. Fu, H. Wang, J. Peng, P. Baxter, C. Hu, and S. Yue, "Angular velocity estimation of image motion mimicking the honeybee tunnel centring behaviour," in *Proc. Int. Joint Conf. Neural Netw. (IJCNN)*, Budapest, Hungary, Jul. 2019, pp. 1–7.
- [15] D. Liu and S. Yue, "Event-driven continuous stdp learning with deep structure for visual pattern recognition," *IEEE Trans. Cybern.*, vol. 49, no. 4, pp. 1377–1390, 2018.
- [16] C. Hu, F. Arvin, C. Xiong, and S. Yue, "Bio-inspired embedded vision system for autonomous micro-robots: the Igmd case," *IEEE Trans. Cogn. Develop. Syst.*, vol. 9, no. 3, pp. 241–254, Sep. 2016.
- [17] Q. Fu, C. Hu, J. Peng, and S. Yue, "Shaping the collision selectivity in a looming sensitive neuron model with parallel on and off pathways and spike frequency adaptation," *Neural Netw.*, vol. 106, pp. 127–143, Oct. 2018.
- [18] M. Mischiati, H.-T. Lin, P. Herold, E. Imler, R. Olberg, and A. Leonardo, "Internal models direct dragonfly interception steering," *Nature*, vol. 517, no. 7534, pp. 333–338, Jan. 2015.
- [19] K. Nordström, P. D. Barnett, and D. C. O'Carroll, "Insect detection of small targets moving in visual clutter," *PLoS Biol.*, vol. 4, no. 3, p. e54, Feb. 2006.
- [20] P. D. Barnett, K. Nordström, and D. C. O'Carroll, "Retinotopic organization of small-field-target-detecting neurons in the insect visual system," *Curr. Biol.*, vol. 17, no. 7, pp. 569–578, Apr. 2007.
- [21] K. Nordström, "Neural specializations for small target detection in insects," *Curr. Opin. Neurobiol.*, vol. 22, no. 2, pp. 272–278, Apr. 2012.
- [22] S. D. Wiederman, J. M. Fabian, J. R. Dunbier, and D. C. O'Carroll, "A predictive focus of gain modulation encodes target trajectories in insect vision," *Elife*, vol. 6, p. e26478, 2017.
- [23] M. F. Keleş and M. A. Frye, "Object-detecting neurons in drosophila," *Curr. Biol.*, vol. 27, no. 5, pp. 680–687, Mar. 2017.
- [24] S. Nicholas, J. Supple, R. Leibbrandt, P. T. Gonzalez-Bellido, and K. Nordström, "Integration of small-and wide-field visual features in target-selective descending neurons of both predatory and nonpredatory dipterans," *J. Neurosci.*, vol. 38, no. 50, pp. 10725–10733, Dec. 2018.
- [25] S. D. Wiederman, P. A. Shoemaker, and D. C. O'Carroll, "A model for the detection of moving targets in visual clutter inspired by insect physiology," *PLoS One*, vol. 3, no. 7, pp. 1–11, Jul. 2008.
- [26] H. Wang, J. Peng, and S. Yue, "A directionally selective small target motion detecting visual neural network in cluttered backgrounds," *IEEE Trans. Cybern.*, vol. 50, no. 4, pp. 1541–1555, Apr. 2020.
- [27] S. D. Wiederman and D. C. O'Carroll, "Biologically inspired feature detection using cascaded correlations of off and on channels," *J. Artif. Intell. Soft Comput. Res.*, vol. 3, no. 1, pp. 5–14, Dec. 2013.
- [28] Z. M. Bagheri, S. D. Wiederman, B. S. Cazzolato, S. Grainger, and D. C. O'Carroll, "Performance of an insect-inspired target tracker in natural conditions," *Bioinspir. & Biomim.*, vol. 12, no. 2, p. 025006, Feb. 2017.
- [29] Z. M. Bagheri, B. S. Cazzolato, S. Grainger, D. C. O'Carroll, and S. D. Wiederman, "An autonomous robot inspired by insect neurophysiology pursues moving features in natural environments," *J. Neural Eng.*, vol. 14, no. 4, p. 046030, Jul. 2017.
- [30] H. Wang, J. Peng, X. Zheng, and S. Yue, "A robust visual system for small target motion detection against cluttered moving backgrounds," *IEEE Trans. Neural Netw. Learn. Syst.*, vol. 31, no. 3, pp. 839–853, Mar. 2020.
- [31] T. C. Kietzmann, C. J. Spoerer, L. K. Sørensen, R. M. Cichy, O. Hauk, and N. Kriegeskorte, "Recurrence is required to capture the representational dynamics of the human visual system," *Proc. Natl. Acad. Sci. U.S.A.*, p. 201905544, Oct. 2019.
- [32] Y. Mohsenzadeh, S. Qin, R. M. Cichy, and D. Pantazis, "Ultra-rapid serial visual presentation reveals dynamics of feedforward and feedback processes in the ventral visual pathway," *Elife*, vol. 7, p. e36329, Jun. 2018.
- [33] E. Tang, M. G. Mattar, C. Giusti, D. M. Lydon-Staley, S. L. Thompson-Schill, and D. S. Bassett, "Effective learning is accompanied by high-dimensional and efficient representations of neural activity," *Nat. Neurosci.*, vol. 22, no. 6, pp. 1000–1009, May 2019.

- [34] A. M. Bastos, J. Vezoli, C. A. Bosman, J.-M. Schoffelen, R. Oostenveld, J. R. Dowdall, P. De Weerd, H. Kennedy, and P. Fries, "Visual areas exert feedforward and feedback influences through distinct frequency channels," *Neuron*, vol. 85, no. 2, pp. 390–401, Jan. 2015.
- [35] S. E. Clarke and L. Maler, "Feedback synthesized neural codes for motion," *Curr. Biol.*, vol. 27, no. 9, pp. 1356–1361, May 2017.
- [36] C. G. Huang, M. G. Metzen, and M. J. Chacron, "Feedback optimizes neural coding and perception of natural stimuli," *ELife*, vol. 7, p. e38935, Oct. 2018.
- [37] G. Li and Y. Yu, "Contrast-oriented deep neural networks for salient object detection," *IEEE Trans. Neural Netw. Learn. Syst.*, vol. 29, no. 12, pp. 6038–6051, Dec. 2018.
- [38] J. Carreira, P. Agrawal, K. Fragkiadaki, and J. Malik, "Human pose estimation with iterative error feedback," in *Proc. IEEE Conf. Comput. Vis. Pattern Recognit.*, 2016, pp. 4733–4742.
- [39] K. Han, H. Wen, Y. Zhang, D. Fu, E. Culurciello, and Z. Liu, "Deep predictive coding network with local recurrent processing for object recognition," in *Proc. Adv. Neural Inf. Process. Syst.*, 2018, pp. 9201–9213.
- [40] C. Cao, Y. Huang, Y. Yang, L. Wang, Z. Wang, and T. Tan, "Feedback convolutional neural network for visual localization and segmentation," *IEEE Trans. Pattern Anal. Mach. Intell.*, vol. 41, no. 7, pp. 1627–1640, Jul. 2019.
- [41] B. Schnell, P. T. Weir, E. Roth, A. L. Fairhall, and M. H. Dickinson, "Cellular mechanisms for integral feedback in visually guided behavior," *Proc. Natl. Acad. Sci. U.S.A.*, vol. 111, no. 15, pp. 5700–5705, Apr. 2014.
- [42] M. Karásek, F. T. Muijres, C. De Wagter, B. D. Remes, and G. C. de Croon, "A tailless aerial robotic flapper reveals that flies use torque coupling in rapid banked turns," *Science*, vol. 361, no. 6407, pp. 1089–1094, Sep. 2018.
- [43] R. Rosner, J. von Hadeln, G. Tarawneh, and J. C. Read, "A neuronal correlate of insect stereopsis," *Nat. Commun.*, vol. 10, no. 1, pp. 1–9, Jun. 2019.
- [44] A. C. Paultk, J. A. Stacey, T. W. Pearson, G. J. Taylor, R. J. Moore, M. V. Srinivasan, and B. Van Swinderen, "Selective attention in the honeybee optic lobes precedes behavioral choices," *Proc. Natl. Acad. Sci. U.S.A.*, vol. 111, no. 13, pp. 5006–5011, Apr. 2014.
- [45] J. C. Tuthill and R. I. Wilson, "Mechanosensation and adaptive motor control in insects," *Curr. Biol.*, vol. 26, no. 20, pp. R1022–R1038, Oct. 2016.
- [46] D. Li, C. P. Chen, Y.-J. Liu, and S. Tong, "Neural network controller design for a class of nonlinear delayed systems with time-varying full-state constraints," *IEEE Trans. Neural Netw. Learn. Syst.*, vol. 30, no. 9, pp. 2625–2636, Jan. 2019.
- [47] D. Ding, Z. Wang, Q.-L. Han, and G. Wei, "Neural-network-based output-feedback control under round-robin scheduling protocols," *IEEE Trans. Cybern.*, vol. 49, no. 6, pp. 2372–2384, Jun. 2019.
- [48] L. Liu, Y.-J. Liu, and S. Tong, "Neural networks-based adaptive finite-time fault-tolerant control for a class of strict-feedback switched nonlinear systems," *IEEE Trans. Cybern.*, vol. 49, no. 7, pp. 2536–2545, Jul. 2019.
- [49] A. Meglić, M. Ilić, P. Pirih, A. Škorjanc, M. F. Wehling, M. Kreft, and G. Belušić, "Horsefly object-directed polarotaxis is mediated by a stochastically distributed ommatidial subtype in the ventral retina," *Proc. Natl. Acad. Sci. U.S.A.*, p. 201910807, Oct. 2019.
- [50] R. Behnia, D. A. Clark, A. G. Carter, T. R. Clandinin, and C. Desplan, "Processing properties of on and off pathways for drosophila motion detection," *Nature*, vol. 512, no. 7515, p. 427, Aug. 2014.
- [51] S.-y. Takemura, A. Bhatiroke, Z. Lu, A. Nern, S. Vitaladevuni, P. K. Rivilin, W. T. Katz, D. J. Olbris, S. M. Plaza, P. Winston *et al.*, "A visual motion detection circuit suggested by drosophila connectomics," *Nature*, vol. 500, no. 7461, p. 175, Aug. 2013.
- [52] B. De Vries and J. C. Príncipe, "A theory for neural networks with time delays," in *Proc. NIPS*, 1990, pp. 162–168.
- [53] B. Gulyas, G. Orban, J. Duyssens, and H. Maes, "The suppressive influence of moving textured backgrounds on responses of cat striate neurons to moving bars," *J. Neurophysiol.*, vol. 57, no. 6, pp. 1767–1791, Jun. 1987.
- [54] A. C. Paultk, L. Kirszenblat, Y. Zhou, and B. van Swinderen, "Closed-loop behavioral control increases coherence in the fly brain," *J. Neurosci.*, vol. 35, no. 28, pp. 10 304–10 315, Jul. 2015.
- [55] E. M. Crowe, C. J. Howard, A. S. Attwood, and C. Kent, "Goal-directed unequal attention allocation during multiple object tracking," *Atten. Percept. Psychophys.*, vol. 81, no. 5, pp. 1312–1326, Jul. 2019.
- [56] A. D. Straw, "Vision egg: an open-source library for realtime visual stimulus generation," *Front. Neuroinf.*, vol. 2, no. 4, Nov. 2008.
- [57] *RIST Data Set*. [Online], Available: <https://sites.google.com/view/hongxinwang-personalsite/download>, accessed Apr. 6, 2020.
- [58] B. Kimmerle and M. Egelhaaf, "Detection of object motion by a fly neuron during simulated flight," *J. Comp. Physiol. A*, vol. 186, no. 1, pp. 21–31, Jan. 2000.
- [59] A. Cao and P. H. Schiller, "Neural responses to relative speed in the primary visual cortex of rhesus monkey," *Vis. Neurosci.*, vol. 20, no. 1, pp. 77–84, Jan. 2003.
- [60] D. Tadin, W. J. Park, K. C. Dieter, M. D. Melnick, J. S. Lappin, and R. Blake, "Spatial suppression promotes rapid figure-ground segmentation of moving objects," *Nat. Commun.*, vol. 10, no. 1, pp. 1–12, Jul. 2019.